MATERIALS SCIENCE

Peptide framework for screening the effects of amino acids on assembly

Seren Hamsici[1], Andrew D. White[2]*, Handan Acar[1]*

Discovery of peptide domains with unique intermolecular interactions is essential for engineering peptide-based materials. Rather than attempting a brute-force approach, we instead identify a previously unexplored strategy for discovery and study of intermolecular interactions: "co-assembly of oppositely charged peptide" (CoOP), a framework that "encourages" peptide assembly by mixing two oppositely charged hexapeptides. We used an integrated computational and experimental approach, probed the free energy of association and probability of amino acid contacts during co-assembly with atomic-resolution simulations, and correlated them to the physical properties of the aggregates. We introduce CoOP with three examples: dialanine, ditryptophan, and diisoleucine. Our results indicated that the opposite charges initiate the assembly, and the subsequent stability is enhanced by the presence of an undisturbed hydrophobic core. CoOP represents a unique, simple, and elegant framework that can be used to identify the structure-property relationships of self-assembling peptide-based materials.

INTRODUCTION

Self-assembling small peptides are attractive building blocks because they are relatively easy to synthesize and enable systematic study using experimental and computational analyses to associate peptide sequence (structure) with its properties and functionality, making them promising candidates to fabricate functional nanomaterials (*1*). In particular, self-assembly into fibrillar peptide aggregates is abundant in nature and various synthetic technologies in biomedical research (*2*–*9*) and materials science (*10*–*12*). The organization of peptide assemblies emerges from small changes in the amino acid sequence that provides noncovalent interactions, such as electrostatic forces, hydrogen bonds, hydrophobic effects, and aromatic stacking (*13*, *14*). Understanding the effects of these small changes is essential to identify the structure-property relation and create small peptides that do not simply mimic natural sequences but instead are rationally designed for the desired properties. Studies based on editing the peptide sequences of natural designs typically have an initial focus on a particular type of interactions for the property of interest, which may restrict the achievable materials properties (*15*). Screening all possible amino acids to create a wider range of properties, on the other hand, may encounter vast design spaces even for small peptides and is therefore impractical for full experimental exploration. Additional co-assembly strategies are beneficial as they can provide wider optimization of nanomaterials for various applications, but such approaches risk expanding the already vast design space (*1*, *16*). As a result, there is a need for an approach that can bridge the combinatorial explosion of amino acid sequence space with the benefits of editing known sequences to map and search new peptides for new functionalities.

Minimalist peptide designs that incorporate rational modification to produce robust structures have attracted noticable interest over the past two decades (*15*). Diphenylalanine (FF), a motif found in amyloid-β peptides, plays an important role in fiber formation via π-π stacking (*17*). Peptides with an FF motif have spurred the investigation of hierarchical structures and have been used in synthetic materials for various applications from biomedical research to energy harvesting and conversion (*11*, *18*). Consequently, identification of one-dimensional (1D) assembly driven by FF domain has well-established tools that provide standardization and comparison of the results (*19*).

Noncovalent interactions (ranging from 1 to 5 kcal/mol) (*20*) are naturally weak and may not be sufficient for stable and highly ordered assemblies of minimalist peptide designs. To alleviate the low thermodynamic advantage for assembled structures, close proximity (high concentration) in solution is required (kinetic threshold). Addition of hydrophobic groups may provide proximity via spontaneous aggregation in water to assist in assembly, but this approach can reduce or eliminate entirely the solubility of minimalist peptides, which can drastically reduce the utility of any potential application in aqueous environments (*15*). Therefore, a key challenge to the use of traditional minimalist peptides is to address the kinetic threshold for the aggregation.

Here, we overcome the kinetic threshold with enhanced solubility in a hexapeptide, by combining charged and hydrophobic amino acids in a unique design of co-assembling oppositely charged peptides (CoOPs). Because of the relatively small number of interacting groups in a hexapeptide, the kinetic threshold is fairly high. The oppositely charged system addresses this weakness in typical small peptide systems; charges not only assist with aqueous solubility but also provide a relatively long-ranged attractive force to encourage peptides to come together. This effect is analogous to increasing the concentration of peptides without such charged groups.

Here, we introduce the CoOP strategy and explore the effects of alanine (A), tryptophan (W), and isoleucine (I) (we will use the standard single-letter amino acid codes throughout) in this framework. We integrate computational methods to analyze, rather than to predict, the peptide assembly mechanism; atomic-resolution simulations are used to probe the free energy of association and probability of amino acid contact during co-assembly. The effects of the substitution domain on the aggregation kinetics are investigated via pyrene, Congo red staining, and dynamic light scattering (DLS). We use Fourier transform infrared (FTIR) and circular dichroism

[1]Stephenson School of Biomedical Engineering, University of Oklahoma, Norman, OK 73069 USA. [2]Department of Chemical Engineering, University of Rochester, Rochester, NY 14627, USA.
*Corresponding author. Email: andrew.white@rochester.edu (A.D.W.); hacar@ou.edu (H.A.)

to understand the secondary structures of peptides for understanding assembly mechanism and identify the physical properties of the emergent materials via transmission electron microscopy (TEM), atomic force microscopy (AFM), and rheology. We combine the results to understand the relation of peptide sequence, association of intermolecular interactions on assembly kinetics, and structural and mechanical properties of the end products. Here, CoOP is shown to provide a valuable molecular discovery tool that is simple and water soluble and assembles into 1D structure with quantifiable properties for exploring intermolecular interactions and harnessing the rules for peptide assembly phenomena.

RESULTS

CoOP design and validation with molecular dynamics

We have designed a remarkably simple framework composed of soluble hexapeptides that assemble into 1D structures upon mixing via CoOPs (Fig. 1). Hexapeptides are composed of three domains: charged, diphenylalanine (FF), and substitution domain [XX]. The sequences of the co-assembling hexapeptide system are given in Table 1, and chemical structures are in Fig. 1B. The framework sequence remained constant to enable the accurate assessment of the effects of inserting a specific two–amino acid group into the substitution domain, [XX]. As shown in Fig. 1B, the partners of CoOP system have complementary charged amino acids on both ends of the peptides: KFFXXK sequence is the positive partner (pos), and EFFXXE is the negative partner (neg).

Charged amino acids on the peptide termini induce the initial aggregation, followed by subsequent hierarchical assembly of 1D structure that enables screening interactions of substitution domain and applying established methods to compare their effects on the properties of the resulting network. By introducing charged amino acids at both termini of the peptides, we increase solubility and allow the creation of "electrostatic mirror partners" (i.e., peptides with opposite net charge) that enhance aggregation by boosting initial peptide contacts (*21*). We select E and K to provide negative and positive charges, respectively. Our choice is informed by three key observations: First, salt bridges between K and E are known to enhance oligomer stability in β-amyloid peptides (*22*); second, the interaction of R with E is stronger than with K in a very specific direction, providing molecular orientation of binding partners, whereas K salt bridges are effectively isotropic (*23*); last, the additional methylene group of R can contribute nonspecific interactions such as H bonding with the backbone of the partner peptide (*24*, *25*). Acetylation on N termini and amide group on C termini restricts charged interactions to only the amino acid side chains.

The substitution domain ([XX]) in the CoOP system here is designed to be small but displays measurable effects to demonstrate the capabilities of the strategy. We studied dialanine ([AA]), ditryptophan ([WW]), and diisoleucine ([II]), as shown in Fig. 1B, each having a different hydrophobicity index (I > W > A) due to the importance of this parameter for peptide aggregation (*26*, *27*). Hydrophobicity index is related to solvent accessible surface area (ASA), which is defined as the exposed surface area of an amino acid to solvent (*28*). A comparison of the substituted residues based on the ratio of hydrophobic and hydrophilic ASA (ASA ratio) is I (3.9) > W (2.3) > A (1.5) (*29*). Furthermore, the β-sheet propensities of these amino acids that are calculated on the basis of their frequencies of existence in a β-sheet region of analyzed proteins by Chau-Fassman follow a similar trend: I(f:0.274) > W(f:0.203) > A(f:0.167) (*30*).

The assembly pathway and peptide-peptide orientation are defined by the basic molecular framework of CoOP (i.e., the FF domain and terminal charges), while the intermolecular interactions provided by the substitution domain influence the assembly kinetics and mechanism, as well as the physical properties of the hierarchical assembly of the fibrillar structure and its resultant network. As a

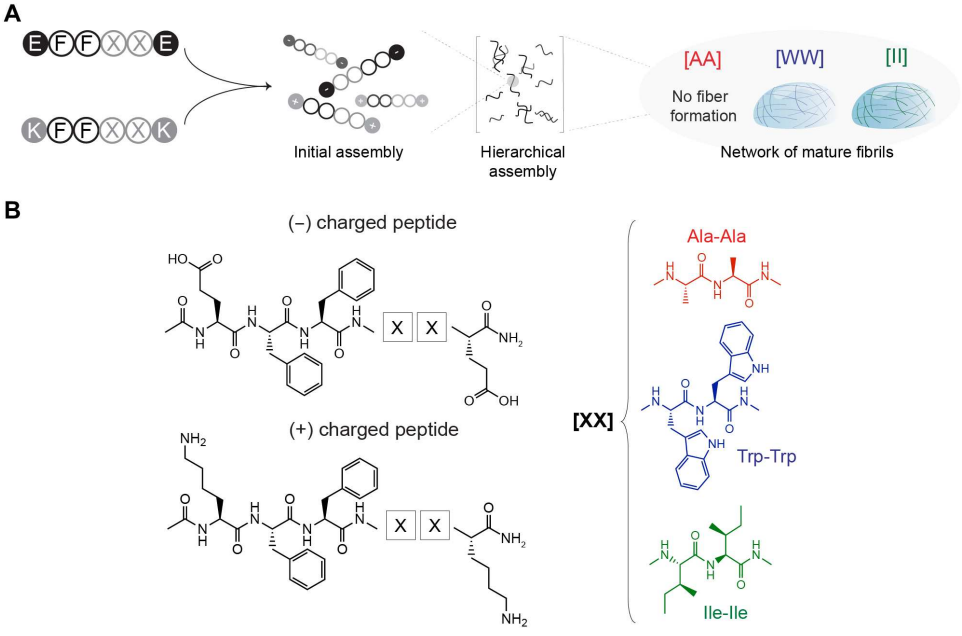

Fig. 1. CoOP design composed of oppositely charged hexapeptide units, which represent the minimalistic assembly template. (**A**) Schematic description of peptide co-assembly triggered by oppositely charged hexapeptides. (**B**) Chemical representation of hexapeptides. E and K residues at both ends provided electrostatic interactions. FF at the core contributed self-assembly with π-π stacking, replacing [XX] with either dialanine, ditryptophan, or diisoleucine to enable tunable hydrophobic interactions.

Table 1. Sequences of the CoOPs used in this study. Each CoOP has negatively and positively charged counterparts.

Nomenclature	(–) charged peptide	(+) charged peptide
[AA]	Ac-EFFAAE-Am	Ac-KFFAAK-Am
[WW]	Ac-EFFWWE-Am	Ac-KFFWWK-Am
[II]	Ac-EFFIIE-Am	Ac-KFFIIK-Am

result, this CoOP system is designed as a tool to screen different canonical and noncanonical amino acids to identify their effects on intermolecular interactions and to correlate them with the initial interactions and properties of the final hydrogel network.

First, we validated the design via molecular dynamics (MD) simulations. All-atom MD was used to access microscopic details that are otherwise difficult to attain in experimental techniques. Specifically, we sought information regarding the initial contact and interactions between amino acid side chains during assembly to assess our design rationale instead of prediction of the entire process. We do not intend the molecular simulations to provide a fully predictive view of the entire process of assembly, as the time and length scales accessible to molecular simulations cannot adequately reproduce experimental systems. Nonetheless, such techniques can help to examine reliability of our initial assumptions about the assembly process and measure free energies of preaggregated peptides.

Enhanced sampling or additional phenomenological modeling must be used to connect the relatively short time scales accessible using MD to the co-assembly experiments. For example, Amirkulova *et al.* (*31*) relied on biasing methods to induce a small four-peptide system to aggregate into structures consistent with experimental nuclear magnetic resonance measurements. Thurston *et al.* (*32*) used Markov state models from all-atom simulations to model the self-assembly of a larger peptide system. Guo *et al.* (*33*) used enhanced sampling methods to understand the dimerization process that nucleates fibrillization in Aβ. Building on this past work, we use enhanced sampling of all-atom simulations to understand the free energy of contacts and initial aggregates of the co-assembly process. Then, we performed unbiased MD to understand the time scales of the peptide interactions. The minimum number of peptides to cover all possible co-assembly interactions is four, and so, all MD contained four peptides (two positives and two negatives). To check whether our conclusions hold to larger systems, we performed unbiased MD of the slowest co-assembling peptide system ([WW]) with 16 peptides for 392 ns (fig. S1).

Free energy surfaces from 500-ns well-tempered metadynamics simulations of the four peptide co-assembling systems are shown in Fig. 2. The collective variables of these free energy surfaces are the average peptide-peptide distance and average intrachain radius of gyration, which correspond to how close the peptides are and how compact they are, respectively. We observed that the order of distances among the pairs in their lowest energy levels (Fig. 2D) is correlated to the order of their ASA ratios and β-sheet propensity constants (Table 2). Hexapeptides with [AA] in the substitution domain showed a close-packed low free energy aggregate state with the least compact peptide structure among the pairs we studied ($R_g \approx 0.48$ nm; Fig. 2A). The distance between [WW] was greater than that of [AA] in their lowest energy levels, but [WW] showed the most compact structures ($R_g \approx 0.35$ to 0.4 nm; see Fig. 2, B and D).

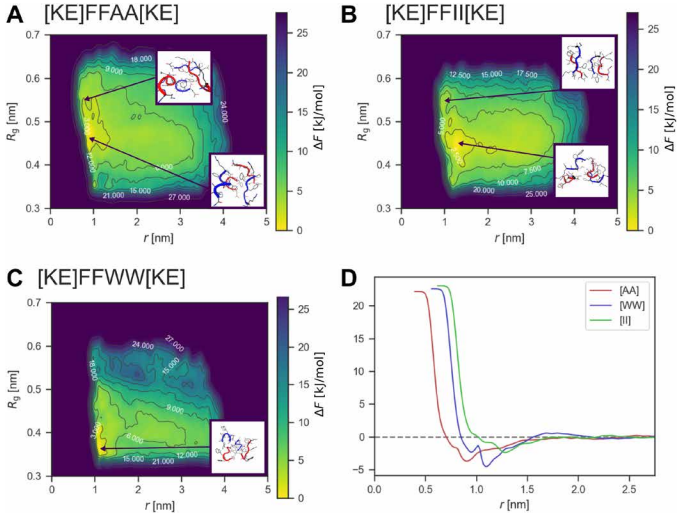

Fig. 2. Free energy surfaces of three co-assembly systems from a metadynamics calculation. Here, *r* is average distance between all centers of mass and R_g is the average radii of gyration (both only consider backbone atoms). (**A** to **C**) Free energy as computed via the metadynamics bias. (**D**) Integrated free energy surface along the average distance. This plot does not predict the occurrence of self-assembly but is instead a measure of solvated peptide aggregation. Figure S2 shows this plot, with pos-pos and neg-neg interactions removed via reweighting. The snapshots show example configurations, with the collective variable values indicated by the arrow.

In [WW], we observed two distinct interactions in the lowest level, cation-π and π-π stacking, which leads to two separate local minima (see Fig. 2D). However, the CoOP system with [II] in the substitution domain showed the greatest separation between peptides in their lowest energy levels, while the side chains were packed closer (as indicated by $R_g \approx 0.43$ nm; see Fig. 2, B and D).

Figure 3 shows the free energy of side-chain contact for peptide pairs between hexapeptides of both same and opposite charges (with contacts defined as a distance ≤3.5 Å). The reference state for these free energies is unbound, resulting in all positive free energies because there is not a single favored conformation for the hexapeptide aggregates. Peptide aggregation is still favored, as seen from Fig. 2D, but no single side-chain contact is found in all aggregate conformations. Tables S1 to S3 show the numerical values with block-averaging uncertainty.

The formation of salt bridges in [AA] is indicated by the favorable free energy for interactions of opposite charges (Fig. 3). Moreover, π-π stacking between F-F also appears to form. However, the hydrophobic core in the region between interacting hexapeptides did not form because of lack of A-A side-chain interactions. The A-A interactions are weaker than the I-I ($P < 10^{-5}$) and W-W interactions ($P < 10^{-10}$), showing that the A-A side-chain interactions contribute little to forming an aggregate hydrophobic core. In addition, as shown in Table 2, the order of β-sheet propensity of these amino acids has a similar trend, which might be decisive in the ordered assembly process after initial aggregation. The [AA] system thus serves as a good control sequence, showing the role of the salt bridge and F-F interactions alone.

Unlike [II], [WW] has relatively favorable neg-neg and pos-pos interactions that are dominated by the interactions of W side chains. The pos-neg interactions involve salt bridges, cation-π, and aromatic W-F interactions. It is important to note that the charged side chains

Table 2. Physical properties of CoOPs. The overall characterization of substitution domains and CAC of their CoOP pairs. N/A, not available.

Substitution domain	Total ASA (*30*)	Hydrophobic ASA (*30*)	Hydrophilic ASA (*30*)	Ratio	Side-chain hydrophobicity index (*26*)	CAC (μM)	β-Sheet frequency (*30*)
A-A	111	66	45	1.5	41	N/A	0.167
W-W	249	174	76	2.3	97	79.4	0.203
I-I	173	137	35	3.9	99	24.5	0.274

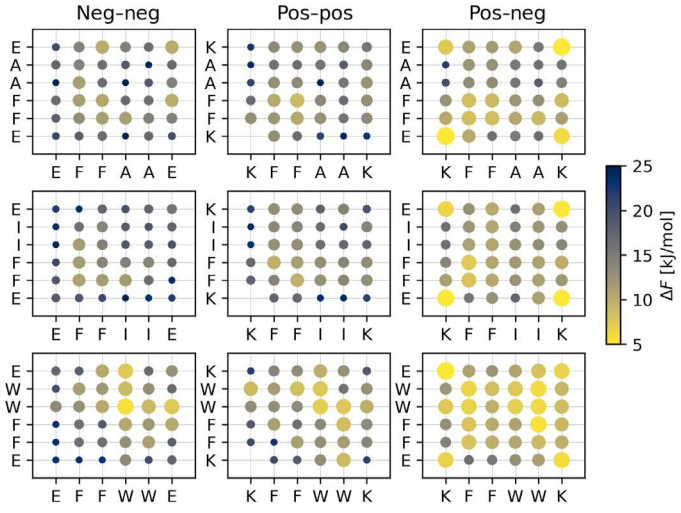

Fig. 3. Free energy of intra- and interchain contact between amino acids. Contact is defined as a pair of two side-chain heavy atoms in an amino acid within 3.5 Å°. These are computed via reweighting the metadynamics simulations (bigger size of circles and lighter color define lower free energy and higher probability of contact).

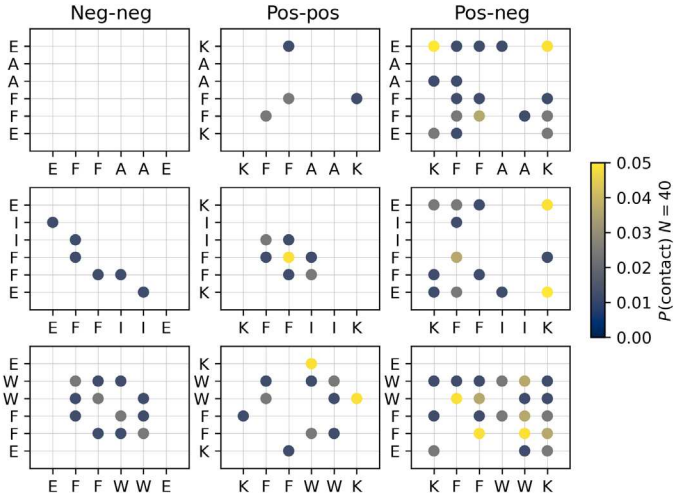

Fig. 4. Probability of first contacting residues from 40 unbiased molecular MDs. Contact is defined as a pair of two side-chain heavy atoms in an amino acid within 3.5 Å°. Simulations ended at a four-chain aggregate and began with the chains at least 2.5 nm apart. Working from the end, this plot shows the minimum nonzero contact maps averaged across the 40 simulations (lighter color represents more contact).

also interact with the core region of [WW] in all alignments, disrupting the core hydrophobicity; for example, K forms interactions with aromatic groups (Fig. 3). The [WW] contact map is qualitatively consistent with the 16-chain system shown in fig. S1, validating the assumption that the enhanced sampling on four chains is a reasonable approximation for larger systems. To understand the probability of first contacting residues in peptide chains, we ran 40 unbiased MD simulations to assess assembly kinetics, with each simulation terminating once all four chains were aggregating. Figure 4 shows the first contact(s) recorded for simulations that resulted in four chains aggregating. These are sampled at a time resolution of 2 ps.

Overall, the [II] and [AA] systems seem to start aggregation frequently with salt bridging. We found the W side chain to be a promiscuous group in the [WW] system, interacting with all residues in the first contacts. These results show that aggregation typically proceeds from pos-neg contact, and this contact can nucleate stable assemblies via either hydrophobic interactions or salt bridging. Such heterogeneous interactions create heterogeneous hierarchical assemblies and so fibrillar structures, as can be seen in TEM of [WW] (Fig. 5B). Figure S3 shows the secondary structure of the three systems at initial contact and gives additional evidence of the heterogeneous nature of the [WW] system. Specifically, the negative chains are helical and the positive chains are β sheet–like.

Perhaps the closest co-assembly modeling work to that described here is the coarse-grained molecular MDs of conjugate acid/base co-assembly of CATCH peptides (*34*). Shao *et al.* (*34*) studied a much larger system and found that co-assembly allows pos-pos and neg-neg pairs as fibers assemble. Regarding the amino acid interactions that drive co-assembly, Frederix *et al.* (*15*) surveyed coarse-grained models of tripeptides and found that the FF motif was a consistently strong influence, as expected from its role in amyloid-β formation (*35*, *36*). The same group also showed that K can be a good choice for a positive amino acid in electrostatically influenced assembly because of its stronger cation-π interactions relative to R.

CoOP assembly and characterization

Upon validation of the design rationale of the CoOP system, we characterized the assembly kinetics and mechanism of the studied pairs experimentally; these aspects are dependent on the substitution domain.

Co-assembly of peptides into 1D structures

The CoOP framework is designed to form 1D aggregations. At pH 7, all peptides were soluble in water and displayed the expected charges [pK_a (where K_a is the acid dissociation constant) of (-COO^-) of E is 4.25 and that of (-NH_3^+) of K is 10.53]. When mixed with equal concentrations and volume, the total charge of the aggregate becomes neutral (fig. S4). Upon simple mixing at room temperature by pipetting, [WW] and [II] rapidly assembled into 1D structures at a

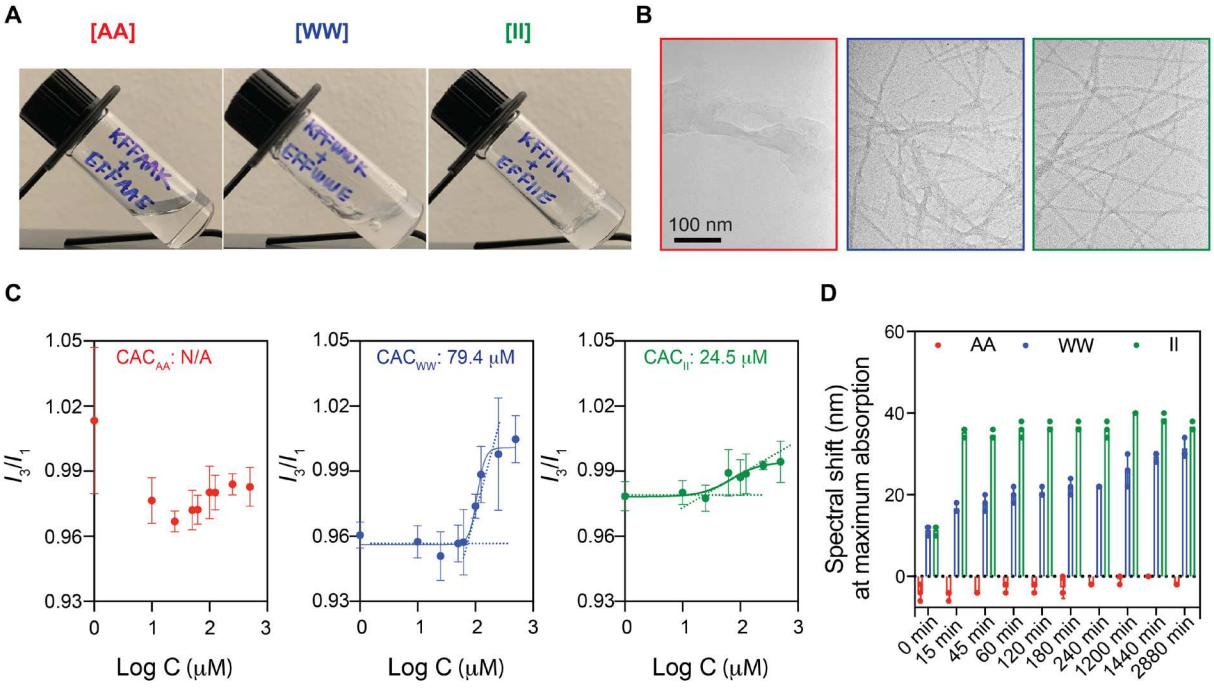

Fig. 5. Hydrogel formation and 1D nanofibrillar assembly kinetics. (**A** and **B**) Upon mixing two oppositely charged peptides, [II] and [WW] formed gels (A) consisting of nanofibers (B), while [AA] did not form any organized structure. (**C**) Molecular co-assembly of the peptides was characterized by CAC determination. (**D**) Characterization of amyloid-like aggregation mechanism probed by Congo red assay for 2 days.

monomer concentration of 10 mM (Fig. 5A) [[AA] = 0.75 weight % (wt %), [WW] = 0.9 wt %, and [II] = 0.8 wt %] without temperature increase, sonication, and pH adjustment. The diameter of the formed 1D nanostructures was measured at around 5 to 10 nm for [II] and [WW] (Fig. 5B and fig. S4). However, for [AA] (featuring the narrowest hydrophobic ASA and the lowest β-sheet frequency), no organized structure was formed at a concentration of 0.75% (w/v), which is lower than previously studied (2%, w/v) (*37*). These results indicate that CoOP meets the three goals of our design rationale: a simple, water-soluble hexapeptide system that assembles into 1D structures when mixed.

Characterization of assembly kinetics and mechanism

The FF domain of the CoOP system provides an amyloid-like 1D assembly that has well-established fluorescence-based analysis methods to compare the assembly kinetics of the system, which is dependent on the substitution domain. Critical aggregation concentration (CAC; the minimal concentration required for the onset of aggregation) was analyzed using the hydrophobic probe pyrene (solubility in water, 2 to 3 μM). Pyrene preferentially aggregates in the interior hydrophobic regions of the assembled structures (*38*). An increase in the ratio of fluorescence intensities of the third and first vibronic peaks of pyrene, I_3/I_1, reveals the hydrophobicity of the local environment; the increased polarity of the local environment reduces the I_3/I_1 ratio. At the CAC, pyrene moves into the hydrophobic inner core and sequesters within the FF domain with a requisite increase in the I_3/I_1 ratio (*39*). Pyrene assay for our CoOP system showed an increase of I_3/I_1 fluorescence intensity ratio for [II] and [WW], indicating 1D structure formation, while no increase for [AA] indicates no assembly at this concentration. Measured I_3/I_1 values were plotted against log values of CoOP monomer concentrations, and sigmoidal hyperbola of the graphs indicates CAC values for [II] and [WW] as 24.50 μM (0.002 wt %) and 79.4 μM (0.007 wt %), respectively (Fig. 5C).

Congo red is an azo dye with a phenyl group, used for characterization of amyloid-like fibrillar assembly, which requires specific orientations of FF domain–derived β sheet–rich structures (*40*). Congo red molecules participate in the fiber assembly process via H bonding and π stacking (*41*). Such arrangement in the fibril assembly causes red shift in Congo red absorption from 498 nm. We observed a red shift in our Congo red analyses for [II] and [WW] (from 498 to 540 nm), but no change was observed for [AA] (Fig. 5D). The red shift for [II] was observed ≈15 min after mixing and remained constant for 48 hours. By contrast, the red shift of [WW] appeared 20 hours after incubation. This indicates that hierarchical assembly into fibrillar structure continues after the initial interactions.

Furthermore, DLS was performed for identification of the concentration when aggregates started to form, instead of measuring the size of the aggregates. When mixed, [AA] and [WW] did not show any aggregates at 25 μM, while the signals of scattered light were observed in [II] in this concentration, which is correlated to the measured CAC of [II], 24.5 μM. The intensity of the scattered light and corresponding aggregate sizes did not increase with increasing concentration of [AA] as expected, because no aggregation is observed for [AA] in these concentrations. [WW] system aggregations showed similar results after 50 μM, due to CAC of [WW] being measured as 79.4 μM. The intensity of the scattered light and its corresponding sizes increased with increasing concentrations for [WW], but no saturation is observed. The intensity of the scattered light increased for larger aggregate sizes for [II] with increasing concentration and oversaturated above 200 μM (i.e., beyond the measurement limits) (Fig. 6).

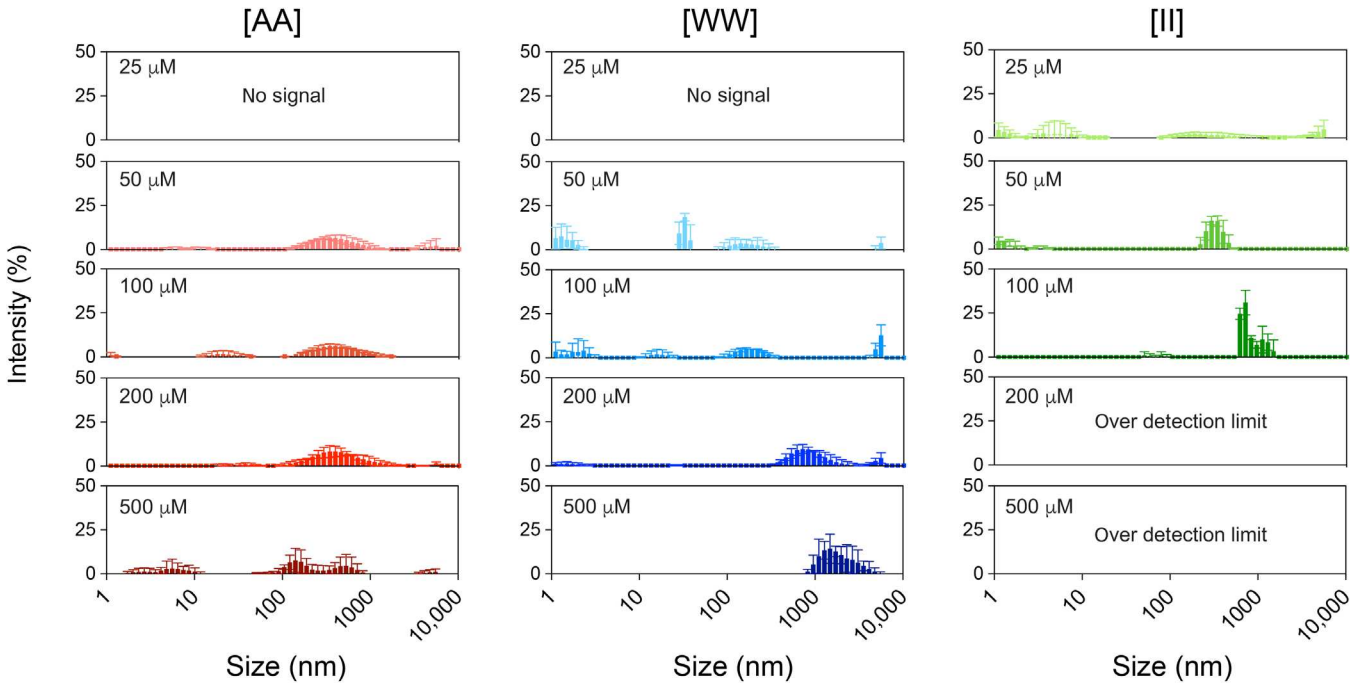

Fig. 6. Determination of aggregation concentration of CoOPs. DLS measurements were performed by co-assembled peptides with immediate incubation.

When the system was incubated overnight, the maturation of the fibrillar structures into network formations, and likewise the intensity of the scattered light in DLS, was enhanced (fig. S8). The aggregates become larger for [AA] after 200 μM, which might indicate some network formation. Similarly, [WW] formed larger aggregates, likely with more uniform size as the intensity of the light increased in a small range of sizes and oversaturated at 500 μM. The saturation concentration is observed at 200 μM for [II] incubated overnight, and the intensity of the scattered light increased in a smaller range for low concentrations.

As expected, the individual peptides alone did not show an observable aggregation at 500 μM, even after overnight incubation (fig. S9). A slight intensity and size changes were observed especially for positively charged groups, in agreement with MD simulation results that indicate that the probability of contact points of positively charged peptides was higher than that of their negatively charged counterparts; however, the intensities were still insufficient to observe a trend with pyrene measurements, and thus, the CAC could not be quantified.

Secondary structure analysis of 1D structures

Directed assembly of CoOP provides analyses of the effect of the substitution domain on the assembly mechanism. Upon initial aggregation, conformational changes of the amino acid side chains create the secondary structures and maturation of the fibrillar assemblies. We analyzed the secondary structures of these systems with FTIR spectroscopy and circular dichroism (CD) under different concentrations.

Amides I and II are two major bands of FTIR analysis for peptide aggregations, as they indicate the conformation of individual peptides. The most sensitive region with regard to a secondary structure is amide I (1600 to 1700 cm^{-1}) as a result of carbonyl (-C═O) stretching of peptide bonds in backbone (*42*). Strong amide I absorption between 1650 and 1655 cm^{-1} is attributed to α-helical structures, while β-sheet structures show a strong absorption band between 1612 and 1640 cm^{-1} (*43*). Amide II results from (-N—H) bending and (-C—N-) stretching (strong band at 1540 to 1550 cm^{-1} with a weaker shoulder at 1510 to 1525 cm^{-1}). FTIR spectrum of [AA] pairs showed a similar trend as in the pyrene and Congo red assays, with no apparent organized assembly at this concentration. The observed broad peak at 1647 cm^{-1} at different [AA] pair concentrations indicates random coil or disorganized structure (Fig. 7A, red). The positive and negative counterparts of [AA] pairs also showed a similar trend (fig. S6). The intensity of the amide I region at 1625 cm^{-1} was observed in [WW] pairs, but this signal was weaker compared to [II] pairs (Fig. 7A, blue). No amide I peak is observed at 50 μM [WW], which is below the CAC (79.4 μM).

The strong band for amide I regions (at 1627 cm^{-1}) of [II] pair FTIR spectrum corresponds to highly ordered peptide assembly (Fig. 7A, green). The next band, occurring at 1545 cm^{-1}, corresponds to amide II regions (N–H bending and C–N stretching, 1450 to 1550 cm^{-1}), which are hardly affected by side-chain vibrations (*44*). While 1 mM [II] showed the strongest intensity in amide I and II regions, the peaks were observable even at 50 μM (CAC [II] is 24.50 μM), indicating that β-sheet structures form at these low concentrations. In addition, individual counterparts of [II] (KFFIIK and EFFIIE) did not show peaks for any concentration studied, even at 1 mM concentration (fig. S6). This suggests that the highly hydrophobic core of this peptide sequence was insufficient to initiate aggregation.

CD provides information regarding the secondary structure of the peptide aggregates. CD spectra for different concentrations of [AA] showed negative peaks at 190 to 200 nm and weak broad shoulders around 217 to 220 nm, which typically indicates unordered or random coil peptide structures (Fig. 7B, red) (*45*). Individual members of [AA] pairs also showed the same trend, indicating no observable ordered structure for these peptides.

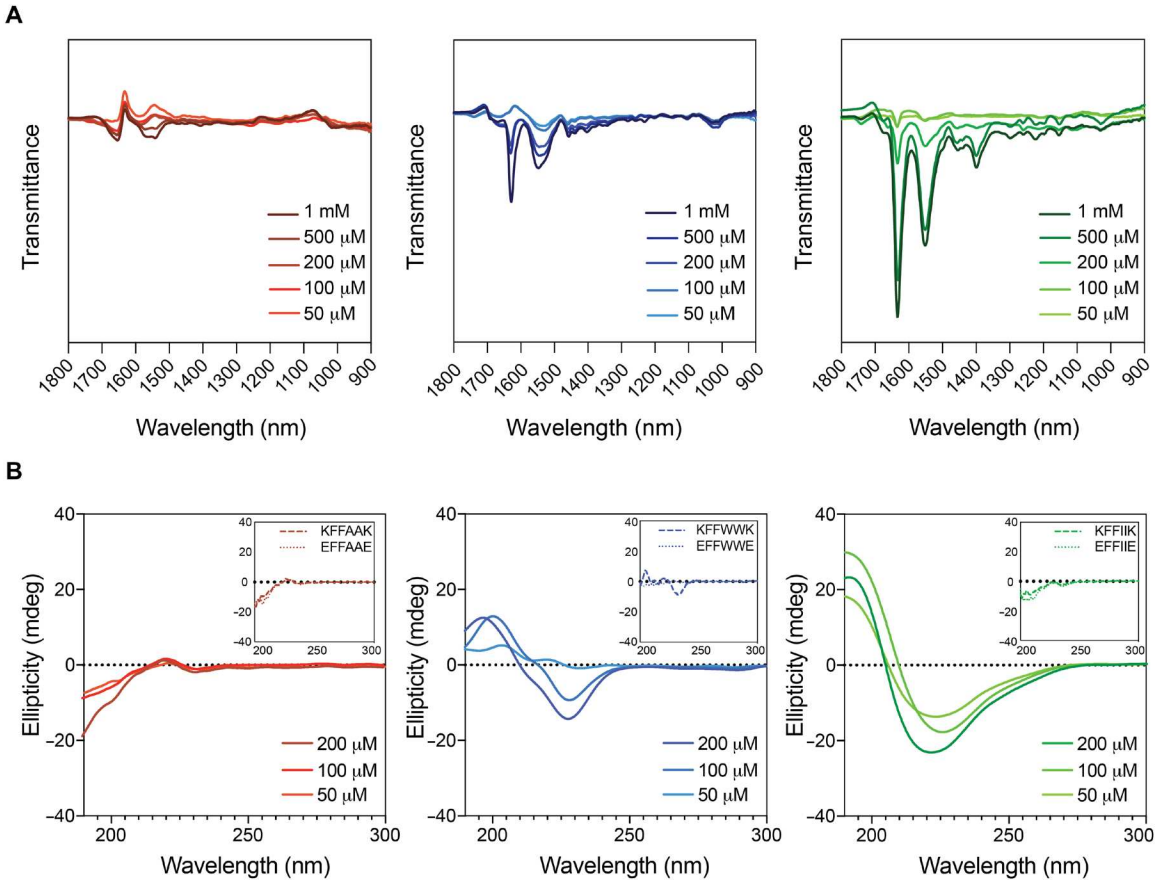

Fig. 7. Structural determination of CoOPs. (**A** and **B**) Secondary structure analysis of CoOPs and the individual counterparts in water with different concentrations by using FTIR and CD measurements.

Peptides with β-sheet conformation typically show broad positive and negative peaks at 195 nm and around 216 to 218 nm, respectively (*1*). [WW] showed a red shift compared to standard β-sheet peaks; a negative peak at 228 nm and a positive peak at 197 nm were observed for 200 μM concentration, with further red shift observed toward 204 nm as the concentration decreases. The resultant shift in CD spectra corresponds to twisted and distorted arrangements, which are known to weaken the intermolecular forces because of increased distances for H bonding (*46*). The observation of weakened structure in CD for [WW] is correlated to their FTIR results. The individual members of the [WW] pair showed opposite trends; while EFFWWE did not show any peak related to structured organization, KFFWWK showed similar two peaks at 195 nm (maximum) and 226 nm (minimum) as in the [WW] pair. The stacking of KFFWWK was also shown by side-chain residues with a high probability of contact in Fig. 3. The stacking of aromatic rings of W shows a negative CD band around 227 nm (*47*). Among the CoOPs in this study, [II] showed the highest positive and negative peaks at 192 and 214 nm with a slight blue shift (2 nm), with all concentrations indicating β sheet–rich structure (Fig. 7B, green) (*1*). As the peptide concentration decreased, slight intensity differences and red shift were observed, indicating the expected weakening of β-sheet content with decreasing concentration (*48*).

Mechanical properties of CoOP systems

The network of 1D structures of CoOP assemblies encapsulates solvent and forms hydrogel at the macro level. The time-dependent mechanical properties of the hydrogels can be correlated to the assembly kinetics and mechanism for each substitution domain. Small-amplitude oscillatory shear rheology measurements enable identification of the shear storage modulus (G'), loss modulus (G''), and loss factor (tan δ), which are all critical hydrogel properties monitored as a function of time, frequency, and applied strain. Peptide-based hydrogels show viscoelastic behaviors. Therefore, we initially identified the linear viscoelastic regime (LVR) for all CoOPs (all 10 mM in water), where the moduli are independent of applied shear strain.

We identified the LVR through a strain sweep for two different time points after mixing the oppositely charged peptides: immediate (Fig. 8) and overnight (20 hours) (fig. S10) incubation. For [II] and [WW], LVR was observed at up to 1% strain, the hydrogel responses (G' and G'') showed independent magnitudes to the changing strain, and hydrogel structure remained intact. After finding the linear region, time sweep scans were performed at 0.1% strain for 20 min, again at immediate and overnight (20-hour) incubation. All peptide groups except [AA] achieved linear regime and showed hydrogel properties ($G'>G''$) in 20 min (Fig. 8). We then analyzed the gelation time where G' and G'' begin to show linear values as strain is applied

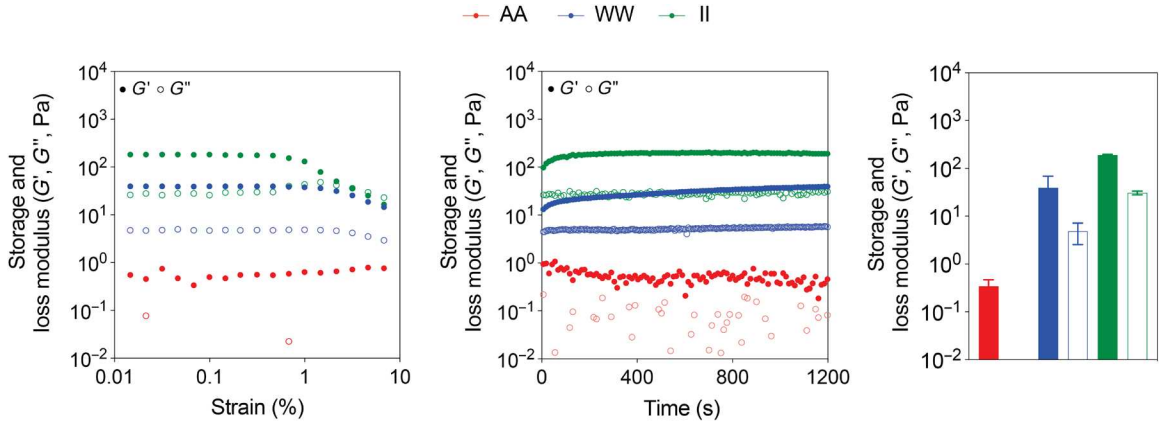

Fig. 8. Mechanical characterization of CoOPs. Time sweep and strain sweep tests of [AA], [WW], and [II] for immediate analysis.

in the LVR. Upon mixing negative and positive counterparts of the CoOP pairs, an immediate increase in G' for [WW] and [II] was observed. We calculated the gelation time by nonlinear fitting of G' data to one-phase association as shown in fig. S7. [II] plateaued only 12 min after mixing according to the fitted data, while [WW] did not plateau during the time of the measurement. The gelation time of [II] is correlated to the kinetics information gathered from Congo red assay, where [II] showed the appropriate intensity in 15 min. [WW] showed continuous assembly over 24 hours in Congo red, also indicated by rheology as G' did not plateau in 20 min. G' [II] was estimated as 192 ±7.3 Pa, nearly three times higher than [WW] (44.5 ±22) in measurements performed immediately upon mixing, and also showed faster gelation. These results indicate stronger and faster aggregation, in agreement with the previous characterization of these systems.

Mechanical properties and time sweep analysis showed that while [II] showed the fastest and strongest gelation behavior, [AA] was found to be the slowest and weakest. These results were also correlated with a Congo red assay, which showed no assembly for [AA], ongoing assembly for [WW], and immediate assembly for [II].

Co-assembly was still ongoing for at least [WW], and thus, we measured the mechanical properties of the CoOPs after incubation at room temperature for an overnight interval (20 hours; fig. S10). The strain sweep analyses showed no substantial change after overnight incubation for assembly of [II] and [WW]. The increased G' value of [AA] indicates some degree of the assembly after 20 hours of incubation. The time sweep measurements revealed more remarkable differences of G' and G'' values for all of the CoOPs at 0.1% strain. G' of [II] increased approximately 3.5× (from 192 ±7.3 Pa to 675 ±55 Pa), indicating a higher degree of assembly after 20 hours. The values for [WW] were more than 8× (from 44.5 ±22 Pa to 453±47.5 Pa). Moreover, [AA] also showed hydrogel properties after overnight assembly (42.5± 5.2 Pa). It is important to note that [WW] showed a steep increase of G' and G'' over time for time sweep analysis after overnight incubation, while the measurements were still in the LVR according to the previous strain sweep test. The reason for this slope might be the orientation of the 1D structures. The immediate measurements were performed directly after the addition of the first negative and then positive counterpart of each pair. However, for overnight incubation at room temperature, the pairs were mixed in an Eppendorf tube. The hydrogels were placed onto the rheology plate with a pipette, which might produce shear thinning of the hydrogel (*49*). A similar increase in G' was also observed for [II] but was not notable compared to [WW] and G' values for the samples plateaued after a short time. In the case of [AA], the G' value was reduced throughout the measurement, which might be due to the loss of weak interactions in [AA].

DISCUSSION

In this study, we introduce CoOPs as a unique and simple molecular discovery tool to identify the effects of intermolecular interactions on the assembly mechanism and mechanical properties of end products. By changing only two amino acids in the appropriate substitution domain of hexapeptides (AA, WW, and II) (Fig. 1), we show marked differences in peptide assembly kinetics, secondary structure, and mechanical properties. The design of this simple molecular framework drives the assembly along a certain pathway, into a 1D structure, to assess, quantify, and compare the effects of different interactions by simple substitutions. There are three important properties of this framework that provide quantification: simplicity, assembly into 1D systems, and water solubility.

The analysis of free energy levels through MD revealed that charged amino acids in this framework enhance the initial peptide aggregation; however, further assembly and stability are derived from interactions among the amino acid side chains in the core of the framework. Among the CoOPs we studied, [AA] side chains do not form a tight solvent-free core in the lowest free energy state (Fig. 2A). This is likely due to the size mismatch of side chains preventing a compact packing of peptides. A similar side-chain size mismatch was shown previously, where co-assembled monomer F and A amino acids phase-separated due to their different intermolecular packing distances (*50*). However, [II] side chains were found to be packed closer in their lowest energy levels (Fig. 2B). This indicates that, at this distance, the side chains of [II] are strongly interacting. Previously, co-assembly of I and F amino acids led to merged structures due to their similar hydrophobicity and side-chain lengths (*50*). Observation of two local minima of distance between [WW] in (Fig. 2) corresponds to cation-π interactions formed at $r \approx 6$ (*51*) and π-π stacking at $r \approx 3.92$ Å (*52*). Furthermore, [WW] showed a slight local peak in the free energy profile at $r \approx 1$ nm that may be due to orientation in π-π stacking. To make the system energetically favorable, the preferred interaction between aromatic rings should be either face to face or edge to face (*53*); however, if two aromatic

rings are different (a heteroaromatic system), the phenol group in the F side chain may interact with the face of a W side chain perpendicularly. Such an arrangement could disrupt the system and lead to a decrease in π-π stacking.

Further analysis of free energy levels was conducted by considering the side chains of individual hexapeptides and co-assembled forms (Fig. 3). For all hexapeptide pairs of the same charge (i.e., either pos-pos or neg-neg), the net charges repel, resulting in higher free energy values (tables S1 to S3). Such repulsion among similar charges correlates with the design rationale for the CoOP system by enhancing the solubility. However, as seen in Fig. 3, even for hexapeptides with the same net charge, the F-F interactions are more favorable, indicating that the addition of more F side chains to the peptides might eventually overcome electrostatic repulsion (a phenomenon known as "molecular frustration") (*54*). The same-charged CoOP system using [WW] showed markedly less favorable F-F interactions than indicated by the [AA] and [II] systems; instead, the interactions between W-W and K-W appeared more favorable. Because there is no salt bridge formation in the same charged groups, this suggests that F-F did not reach the required distance or orientation to provide the low-energy levels seen in other systems. For all groups, the presence of salt bridges appeared to support F-F interactions in co-assembled form as indicated by consistently low energy levels for these interactions compared to [AA] and [II]. All of these observations show the importance of salt bridges in the CoOP system.

The probability of first contacting side-chain residue analysis via MD as shown in Fig. 4 is particularly important as it shows the role of salt chains. In [II] and [AA] systems, the charged residues form the initial interactions. Because of favorable cation-π interactions between the ($-NH_3^+$) of K and high electron density aromatic ring of W (*47*, *51*), the effect of salt bridges is hindered in the [WW] system. In addition, the K side chain produces a relatively weak repulsion compared to E side chain, even when present at both ends of a peptide (*55*), which might also enhance the involvement of K in cation-π interactions. This involvement may reduce salt bridge formation by moderating the interactions between K and E, causing the final co-assembled structure to be more amorphous. Previously, hydrophobic core regions were found to dominate for a "reverse assembly" process and salt bridges were the first to break, indicating that salt bridges are likely not essential for stability after co-assembly (*56*). Here, we find that electrostatic interactions/salt bridges are important to initiate aggregation in the co-assembly of these peptides, but the subsequent assembly and stability are derived from the amino acids in the core of the hexapeptide. As a result, the computational analyses of the free energy levels revealed that the interactions among [AA] are the least favorable compared to [WW] and [II] systems. The ASA trend and β-sheet propensity of chosen amino acids defined the favorability of their CoOP systems, while the initial interactions are likely to happen between the electrostatic groups. The distance between the peptides is inversely correlated to their ASA; the higher the hydrophobicity of the substitution domain amino acid, the longer the distance between the peptides.

The CAC values followed the trend of the distance between the peptides measured in the simulations (Table 2). The closer proximity of the peptides for the formation of interactions requires higher concentrations, while interactions that act over even longer distances are more favorable (as in [II] system). Therefore, the most favorable [II] system showed the lowest CAC, while the least favorable [AA] interactions did not show CAC at the concentrations studied (Fig. 5). As shown in simulations, [AA] requires the closest proximity for the full interactions, which requires higher concentration; the CAC was not observed above 1 mM working conditions. Similarly, the simulations showed [WW] peptides in closer proximity than [II] peptides, as correlated to the narrower hydrophobic ASA of [WW] domain, which resulted in higher CAC concentration than [II]. The kinetics of the assembly of these systems are also relevant to the distance between the interacting peptides, which makes them also more favorable in terms of the free energy differences of the assembled systems. Inevitably, [II] assembles more rapidly than [WW], while [AA] does not assemble into hierarchical order at comparable time scales. The simulation results indicate that interactions between the [AA] peptides might lead to short and instantaneous oligomers instead of large order assemblies without stable β-sheet structure. Furthermore, above the CAC, [II] gave the strongest intensity at 50 and 100 μM within the peptide groups in immediate DLS analysis (Fig. 6). Incubation for overnight (fig. S8) did not change in intensity levels for 50 and 100 μM since the co-assembly of [II] was the highest among other peptide groups and [II] reached the stable state within 15 min as we observed with Congo red assay (Fig. 5D). However, [WW] reached the stable state at 20 hours (Congo red assay), and therefore, we saw a marked increase in DLS measurement of aggregation for overnight incubation (fig. S8). The results of experimental kinetics measurement are found to correlate to the distances between interacting peptides and the thermodynamic free energy measurements, and thus, the experimental and computational analyses are integrated to explain the complex assembly kinetics, demonstrating the advantage of the CoOP system's simple design.

Upon assembly, the [II] system showed ordered β-sheet structures despite the longest distances between the interaction of KFFIIK and EFFIIE (Fig. 7B, green). It can be speculated that the distance between [II] peptides in their lowest energy level might be appropriate for salt bridge formation between K and E, and further favorable conformation of the hydrophobic I side chains. This also suggests that despite the slightly lower free energies and the shorter distance between [AA] and [WW] peptides, they do not form organized assemblies as [II] does at this low concentration. However, more studies are necessary to add further support for this speculation.

Last, the connection between the mechanical properties of the assembled end products and the results of the MD analyses is identified with the CoOP system. Analyses were performed immediately upon mixing the peptides to show the effects of the initial interactions over mechanical properties, which was also studied in MD simulations. The trend of the mechanical properties measured in the experiment was similar to the MD results and to previous characterizations: [II] showed the fastest assembly and highest storage modulus upon mixing, followed by [WW], while [AA] did not show a hydrogel formation at this concentration. Overnight incubation increased the mechanical properties of all systems, including [AA], which shows that the systems were dynamic and assembly was continued, but the amplitude of change was still lowest for [II] system, showing that the conformation of the peptides in this system occurs fastest. The MD simulations indicate that the initial interactions (electrostatic, in these examples) are necessary for aggregation. The assembly into fibrillar structures requires conformational changes of the side chains of the amino acids in the core, as well as hierarchical assembly of the fibrils. All of these assemblies are time dependent and affect the length of the fibrils and their entanglement, and thus the mechanical properties of the overall structure. The enhanced mechanical

properties of the network after overnight incubation at room temperature indicate time-dependent enhancement of the fibrillar and network structure, and thus the thermodynamic influences on this self-assembly (Fig. 8 and fig. S10) As such, the time has a strong effect on fibrillar maturation (Fig. 6 and fig. S8).

The hydrophobic ASA directly affects the interactions between the peptides (the lowest free energy and assembly kinetics), structural organizations (ordered β sheet), and mechanical properties. Moreover, these results highlight the importance of salt bridges on stability in mechanical properties; [II] has the opposite charges around the hydrophobic core, and the charges interact with each other rather than the hydrophobic core amino acids. In the [WW] case, the charges also interact and disrupt the hydrophobic core and making [WW] harder to stabilize, thus changing the mechanical properties dramatically. This effect can also be seen in individual DLS measurements (fig. S9). In the immediate analysis, KFFWWK was the only group that resulted in the highest aggregation level. Furthermore, TEM and AFM images of [WW] showed more heterogeneous fibrillar structures. Therefore, an undisrupted hydrophobic core was shown to be an important parameter for establishing the assembly in CoOP, while charges around the hydrophobic region enhance the stability.

In this study, we introduced a new approach to analyze the intermolecular interactions by combining computational simulations and experimental methods. We leverage MD to reveal information on the initial interactions between peptide side chains at a molecular level to confirm our design principles rather than "predicting" the entire assembly process. Without appropriate sampling, the full time and length scale of the molecular simulations cannot fully reproduce the experimental systems. The rapid assembly process of CoOP systems is a problem for practical experimental sampling, but analysis of the initial interactions via MD confirmed our design rationale for the addition of charged peptides on both sides. Moreover, this approach enables the discovery of new peptide sequences and functionalities by combining both screening and editing of various amino acids with MD and experimental techniques. The strategy we describe here provides screening of both natural and noncanonical amino acids in a special substitution domain of the predetermined assembly framework, where the kinetics and assembly mechanism are dependent on the substitution domain.

Applications of peptide-based nanostructures are growing, and it is therefore valuable to combine experimental, theoretical, and computational methods to explore and define structure-property relationships (*57*). A fundamental understanding of intermolecular interactions is the key to engineer complex soft materials that translate effectively from laboratory conditions into everyday life (*18*). A simple, carefully designed peptide platform that can deconvolute the otherwise complicated influence of noncovalent interactions on bulk material properties will therefore provide an important tool for molecular engineering. In this regard, the CoOP system is a minimalist approach (experimentally and computationally) for peptide assembly studies. CoOP provides a flexible and robust platform to study and compare the effects of intermolecular interactions and correlates the computational thermodynamic and experimental kinetic analyses to mechanical properties. Therefore, our results can provide the foundation for engineering peptides to produce soft materials with desired and predictable properties. CoOP thus has the potential to pave the way for a materials genome atlas for peptide-based materials (*57*).

MATERIALS AND METHODS

Materials

Congo red dye and pyrene were purchased from Sigma-Aldrich. Deionized water (resistance of 18.2 megohm·cm) was used during the experiments. Peptides were purchased from Biomatik Corporation (Canada) with higher than 95% purity.

CAC determination

CAC of peptides was examined using pyrene based on previously published procedures with slight modifications (*58*). Aliquots of pyrene solutions (225 μM in acetone, 4 μl) were added to positively charged peptides (500, 250, 125, 62.5, 31.25, 15.6, 7.81, and 3.9 μM) before the addition of negatively charged peptides (500, 250, 125, 62.5, 31.25, 15.6, 7.81, and 3.9 μM). The inal pyrene concentration in the system was 4.5 μM in microplates. Solutions were left for 30 min to reach equilibrium. Excitation was carried out at 334 nm, and emission spectra were recorded ranging from 360 to 600 nm with a microplate reader (BioTek Neo2SM). Both excitation and emission bandwidths were 9 nm. From the pyrene emission spectra, the fluorescence intensity ratio of the vibronic bands (I_{397}/I_{380}) was plotted against the logarithm of the concentration of the self-assembled peptides. Fitting of the dataset was performed with a model of four-parameter logistic curve by using GraphPad Prism 9.0.0. Then, CAC value was calculated from the intersection of the tangents.

Congo red assay

Congo red assay is used for amyloid fibril detection. In the presence of high β-sheet organization, Congo red lies parallel to the fibril axis and induces a red shift in the absorption maximum (498 nm). Congo red dye was dissolved in water to a final concentration of 500 μM. For sample preparation, stock peptides in water (10 mM) were diluted to 1 mM in water. Then, 1 mM of negative peptide (50 μl) was added to 96-well black plate, and then 1 mM positively charged peptide (50 μl) was added to the same place. A total of 2 μl of 500 μM Congo red was immediately added to the solution and read with a microplate reader (BioTek Neo2SM) at room temperature; spectral scanning for absorbance was adjusted between 400 and 600 nm. The control group of only Congo red dye in water was also prepared with a final concentration of 10 μM. The analysis was performed for 2 days with 10 time points. Spectral shift was calculated on the basis of Congo red–only absorption maximum.

DLS measurements

Hydrodynamic size and ζ potential of single and mixed peptides were measured by DLS. A ZetaSizer Nano ZS (Malvern, UK) instrument with a detector angle of 173° was used for analysis. Clear disposable cell cuvettes were first washed three times with 0.22-μm filtered deionized water (resistance of 18.2 megohm·cm). Before measurements, peptide solutions in phosphate-buffered saline were also filtered with a 0.22-μm filter to avoid any dust that can alter the measurements. For individual peptides, 500 μM (500 μl) positively and negatively charged peptides were used. For mixed peptides, equimolar (500, 200, 100, 50, and 25 μM with 200) of positively (250 μl) and negatively (250 μl) charged peptides was mixed. The analysis was performed with three scans and 21 measurements in each scan.

Rheology measurements

Rheology measurements of 10 mM samples at pH 7 were performed to understand the mechanical properties of the resulting gels. At

rheometer stage, first negatively charged and then positively charged peptide was added, and then an immediate analysis was performed. For overnight analysis, 10 mM equal volumes (200 μl each) of oppositely charged peptides were mixed in Eppendorf tubes and incubated at room temperature overnight (21 hours). The total volume of samples was 200 μl (100 μl of positively charged and 100 μl of negatively charged peptide). A Discovery Hybrid Rheometer-2 rheometer (TA Instruments, New Castle, DE) equipped with parallel 20-mm plate was used for the analysis. Measuring distance was determined as 0.5 mm. Time sweep tests of each sample were carried out for 20 min. Angular frequency and strain magnitudes were determined as $\omega = 10$ rad/s and $\gamma = 0.1\%$, respectively. To determine linear viscoelastic region, amplitude sweep tests of 10 mM samples at pH 7 were performed in the same configuration and concentration. Strain value logarithmically increased from 0.1 to 10%; a total of 17 values were measured. Angular frequency was kept as constant at $\omega = 10$ rad/s.

FTIR and CD measurements

Peptides with different concentrations (1000, 500, 200, 100, and 50 μM) were prepared in water, and analysis was performed immediately. For [AA], [WW], and [II] groups, equal volumes of charged peptides were mixed (as a total of 20 μl) and put directly into FTIR stage. Analysis was performed with Bruker Tensor II with BioATR II unit. For background spectrum, water was measured first, and then peptides in water were subtracted automatically in the device. Analysis was performed between 1800 and 900 cm^{-1}, with 4-cm^{-1} resolution and 60 scans. For CD measurements, analysis was performed in water with a concentration of 200, 100, and 50 μM for co-assembled peptides and 200 μM for individual peptides with a volume of 1 ml. Jasco J-715 was used to collect spectra from 190 to 400 nm, with 0.1-nm data pitch and bandwidth arranged as 1.0 nm.

AFM measurements

Peptide samples were prepared by dilution of 10 mM of co-assembled samples to 0.2 mM with water. Then, 20 μl of diluted peptide samples was dropped onto silicon wafer and dried at room temperature. Topographic imaging was performed in contact mode using an Asylum Research MFP-3D AFM with an Asylum Research cantilever probe (model: TR400PB, lot number: 3733FB). Scanning frequency was 2 kHz, and data points were taken in a 128 × 128 grid over 3 μm–by–3 μm area.

Molecular dynamics

MD calculations used GROMACS 2020.03 (*59*–*65*) as driven by GromacsWrapper (*66*). The CHARMM27 force field was used for modeling the peptides because it has good parameters for acetylated and amidated N/C termini (*67*, *68*). A time step of 2 fs was used to integrate the forces, and simulations were performed in the NVT ensemble using the canonical sampling through velocity rescaling thermostat (*69*). Long-range electrostatic forces were calculated with the particle mesh Ewald method (*70*). Shifted van der Waals and short-range electrostatics were used with a cutoff distance of 1 nm. Hydrogen-containing covalent bonds were constrained using the LINear Constraint Solver (LINCS) algorithm (*71*). Initial structures of peptides were generated with PeptideBuilder (*72*), and Packmol was used to pack together multiple peptide chains into a single coordinate file under the constraint that peptides were at least 2.5 nm apart (*73*). Water and NaCl counterions were added to reach a peptide concentration of 25 mg/ml and a salt concentration of 10 mM. Although the concentration is relatively high, Thota *et al.* (*74*) found that the aggregation thermodynamics are relatively independent of box size. The PLUMED2 package was used to calculate radii of gyration and center of mass distances and to perform metadynamics enhanced sampling (*75*, *76*). MDTraj was used to compute contact maps (*77*), which were reweighed to account for the metadynamics bias (*78*).

All systems were energy-minimized. Metadynamics simulations were additionally equilibrated for 2 ns in the Berendsen isotropic NPT ensemble. Unbiased simulation used for kinetics analysis was run until all four peptide chains had a center of mass distance of less than 1.25 nm among their closest neighbors (≈5 to 50 ns). Metadynamics simulations were run for 500 ns. The 16-peptide chain WW simulations were run for 392 ns. Metadynamics simulations were biased with the enhanced sampling well-tempered metadynamics method (*79*, *80*) with a bias factor of 5, a pace of 1 ns, and a hill height of 5 kJ/mol. The biased collective variables are average center of mass distances between chains ($\sigma = 0.05$ nm) and average radius of gyration of the chains ($\sigma = 0.01$ nm), with only backbone atoms considered.

SUPPLEMENTARY MATERIALS

Supplementary material for this article is available at https://science.org/doi/10.1126/sciadv.abj0305

REFERENCES AND NOTES

1. W. Ji, C. Yuan, P. Chakraborty, P. Makam, S. Bera, S. Rencus-Lazar, J. Li, X. Yan, E. Gazit, Coassembly-induced transformation of dipeptide amyloid-like structures into stimuli-responsive supramolecular materials. *ACS Nano* **14**, 7181–7190 (2020).
2. H. Acar, S. Srivastava, E. Chung, M. Schnorenberg, J. Barrett, J. LaBelle, M. Tirrell, Self-assembling peptide-based building blocks in medical applications. *Adv. Drug Deliv. Rev.* **110-111**, 65–79 (2017).
3. K. J. Nagy, M. C. Giano, A. Jin, D. J. Pochan, J. P. Schneider, Enhanced mechanical rigidity of hydrogels formed from enantiomeric peptide assemblies. *J. Am. Chem. Soc.* **133**, 14975–14977 (2011).
4. D. Wu, N. Sinha, J. Lee, B. P. Sutherland, N. I. Halaszynski, Y. Tian, J. Caplan, H. V. Zhang, J. G. Saven, C. J. Kloxin, D. J. Pochan, Polymers with controlled assembly and rigidity made with click-functional peptide bundles. *Nature* **574**, 658–662 (2019).
5. S. Hamsici, M. Sardan Ekiz, G. Cinar Ciftci, A. B. Tekinay, M. O. Guler, Gemcitabine integrated nano-prodrug carrier system. *Bioconjug. Chem.* **28**, 1491–1498 (2017).
6. G. Cinar, A. Ozdemir, S. Hamsici, G. Gunay, A. Dana, A. B. Tekinay, M. O. Guler, Local delivery of doxorubicin through supramolecular peptide amphiphile nanofiber gels. *Biomater. Sci.* **5**, 67–76 (2017).
7. G. Gunay, M. Sardan Ekiz, X. Ferhati, B. Richichi, C. Nativi, A. B. Tekinay, M. O. Guler, Antigenic GM3 lactone mimetic molecule integrated mannosylated glycopeptide nanofibers for the activation and maturation of dendritic cells. *ACS Appl. Mater. Interfaces* **9**, 16035–16042 (2017).
8. G. Gunay, M. Sever, A. B. Tekinay, M. O. Guler, Three-dimensional laminin mimetic peptide nanofiber gels for in vitro neural differentiation. *Biotechnol. J.* **12**, 1–9 (2017).
9. S. Hamsici, G. Cinar, A. Celebioglu, T. Uyar, A. B. Tekinay, M. O. Guler, Bioactive peptide functionalized aligned cyclodextrin nanofibers for neurite outgrowth. *J. Mater. Chem. B* **5**, 517–524 (2017).
10. E. Gazit, Reductionist approach in peptide-based nanotechnology. *Annu. Rev. Biochem.* **87**, 533–553 (2018).
11. H. Acar, R. Garifullin, L. E. Aygun, A. K. Okyay, M. O. Guler, Amyloid-like peptide nanofiber templated titania nanostructures as dye sensitized solar cell anodic materials. *J. Mater. Chem. A* **1**, 10979–10984 (2013).
12. H. Acar, R. Genc, M. Urel, T. S. Erkal, A. Dana, M. O. Guler, Self-assembled peptide nanofiber templated one-dimensional gold nanostructures exhibiting resistive switching. *Langmuir* **28**, 16347–16354 (2012).
13. S. Hamsici, G. Gunay, H. Kirit, A. Kamatar, K. Loving, H. Acar, Chapter 9—Drug delivery applications of peptide materials, in *Peptide-Based Biomaterials* (The Royal Society of Chemistry, 2021), pp. 291–334.
14. M. J. Webber, E. T. Pashuck, (Macro)molecular self-assembly for hydrogel drug delivery. *Adv. Drug Deliv. Rev.* **172**, 275–295 (2021).

15. P. Frederix, G. Scott, Y. Abul-Haija, D. Kalafatovic, C. Pappas, N. Javid, N. Hunt, R. Ulijn, T. Tuttle, Exploring the sequence space for (Tri-)peptide self-assembly to design and discover new hydrogels. *Nat. Chem.* **7**, 30–37 (2015).
16. S. Fleming, S. Debnath, P. W. J. M. Frederix, N. T. Hunt, R. V. Ulijn, Insights into the coassembly of hydrogelators and surfactants based on aromatic peptide amphiphiles. *Biomacromolecules* **15**, 1171–1184 (2014).
17. E. Gazit, A possible role for π-stacking in the self-assembly of amyloid fibrils. *FASEB J.* **16**, 77–83 (2002).
18. G. Wei, Z. Su, N. P. Reynolds, P. Arosio, I. W. Hamley, E. Gazit, R. Mezzenga, Self-assembling peptide and protein amyloids: From structure to tailored function in nanotechnology. *Chem. Soc. Rev.* **46**, 4661–4708 (2017).
19. A. Aliyan, N. P. Cook, A. A. Martí, Interrogating amyloid aggregates using fluorescent probes. *Chem. Rev.* **119**, 11819–11856 (2019).
20. H. Lodish, A. Berk, S. L. Zipursky, P. Matsudaira, D. Baltimore, J. Darnell, Noncovalent bonds, in *Molecular Cell Biology* (WH Freeman, ed. 4, 2000).
21. Z. Zeravcic, V. N. Manoharan, M. P. Brenner, Size limits of self-assembled colloidal structures made using specific interactions. *Proc. Natl. Acad. Sci. U.S.A.* **111**, 15918–15923 (2014).
22. D. Klimov, D. Thirumalai, Dissecting the assembly of Aβ16–22 amyloid peptides into antipar-allel β sheets. *Structure* **11**, 295–307 (2003).
23. A. D. White, A. J. Keefe, J.-R. Ella-Menye, A. K. Nowinski, Q. Shao, J. Pfaendtner, S. Jiang, Free energy of solvated salt bridges: A simulation and experimental study. *J. Phys. Chem. B* **117**, 7254–7259 (2013).
24. A. Jalan, J. Hartgerink, Pairwise interactions in collagen and the design of heterotrimeric helices. *Curr. Opin. Chem. Biol.* **17**, 960–967 (2013).
25. J. Banerjee, H. Azevedo, Crafting of functional biomaterials by directed molecular self-assembly of triple helical peptide building blocks. *Interface Focus* **7**, 20160138 (2017).
26. O. D. Monera, T. J. Sereda, N. E. Zhou, C. M. Kay, R. S. Hodges, Relationship of sidechain hydrophobicity and α-helical propensity on the stability of the single-stranded amphipathic α helix. *J. Pept. Sci.* **1**, 319–329 (1995).
27. Y. Mu, M. Yu, Effects of hydrophobic interaction strength on the self-assembled structures of model peptides. *Soft Matter* **10**, 4956–4965 (2014).
28. R. Heffernan, K. Paliwal, J. Lyons, A. Dehzangi, A. Sharma, J. Wang, A. Sattar, Y. Yang, Y. Zhou, Improving prediction of secondary structure, local backbone angles and solvent accessible surface area of proteins by iterative deep learning. *Sci. Rep.* **5**, 11476 (2015).
29. L. Lins, A. Thomas, R. Brasseur, Analysis of accessible surface of residues in proteins. *Protein Sci.* **12**, 1406–1417 (2003).
30. P. Y. Chou, G. D. Fasman, Conformational parameters for amino acids in helical, β-sheet, and random coil regions calculated from proteins. *Biochemistry* **13**, 211–222 (1974).
31. D. B. Amirkulova, M. Chakraborty, A. D. White, Experimentally consistent simulation of aβ21–30 peptides with a minimal NMR bias. *J. Phys. Chem. B* **124**, 8266–8277 (2020).
32. B. A. Thurston, J. D. Tovar, A. L. Ferguson, Thermodynamics, morphology, and kinetics of early-stage self-assembly of π-conjugated oligopeptides. *Mol. Simul.* **42**, 955–975 (2016).
33. A. Z. Guo, A. M. Fluitt, J. J. de Pablo, Early-stage human islet amyloid polypeptide aggregation: Mechanisms behind dimer formation. *J. Chem. Phys.* **149**, 025101 (2018).
34. Q. Shao, K. M. Wong, D. T. Seroski, Y. Wang, R. Liu, A. K. Paravastu, G. A. Hudalla, C. K. Hall, Anatomy of a selectively coassembled β-sheet peptide nanofiber. *Proc. Natl. Acad. Sci. U.S.A.* **117**, 4710–4717 (2020).
35. N. Kol, L. Adler-Abramovich, D. Barlam, R. Z. Shneck, E. Gazit, I. Rousso, Self-assembled peptide nanotubes are uniquely rigid bioinspired supramolecular structures. *Nano Lett.* **5**, 1343–1346 (2005).
36. X. Yan, P. Zhu, J. Li, Self-assembly and application of diphenylalanine-based nanostructures. *Chem. Soc. Rev.* **39**, 1877–1890 (2010).
37. G. Cinar, H. Ceylan, M. Urel, T. S. Erkal, E. Deniz Tekin, A. B. Tekinay, A. Dâna, M. O. Guler, Amyloid inspired self-assembled peptide nanofibers. *Biomacromolecules* **13**, 3377–3387 (2012).
38. K. Kalyanasundaram, J. Thomas, Environmental effects on vibronic band intensities in pyrene monomer fluorescence and their application in studies of micellar systems. *J. Am. Chem. Soc.* **99**, 2039–2044 (1977).
39. V. Castelletto, I. W. Hamley, Self assembly of a model amphiphilic phenylalanine peptide/polyethylene glycol block copolymer in aqueous solution. *Biophys. Chem.* **141**, 169–174 (2009).
40. C. Wu, J. Scott, J.-E. Shea, Binding of congo red to amyloid protofibrils of the alzheimer Aβ9–40 peptide probed by molecular dynamics simulations. *Biophys. J.* **103**, 550–557 (2012).
41. A. Howie, D. Brewer, Optical properties of amyloid stained by Congo red: History and mechanisms. *Micron* **40**, 285–301 (2009).
42. M. Hughes, P. Frederix, J. Raeburn, L. Birchall, J. Sadownik, F. Coomer, I.-H. Lin, E. Cussen, N. Hunt, T. Tuttle, S. Webb, D. Adams, R. Ulijn, Sequence/structure relationships in aromatic dipeptide hydrogels formed under thermodynamic control by enzyme-assisted self-assembly. *Soft Matter* **8**, 5595–5602 (2012).
43. J. Pelton, L. McLean, Spectroscopic methods for analysis of protein secondary structure. *Anal. Biochem.* **277**, 167–176 (2000).
44. A. Barth, C. Zscherp, What vibrations tell about proteins. *Q. Rev. Biophys.* **35**, 369–430 (2002).
45. R. Gopal, J. S. Park, C. H. Seo, Y. Park, Applications of circular dichroism for structural analysis of gelatin and antimicrobial peptides. *Int. J. Mol. Sci.* **13**, 3229–3244 (2012).
46. D. E. Clarke, C. D. J. Parmenter, O. A. Scherman, Tunable pentapeptide self-assembled β-sheet hydrogels. *Angew. Chem. Int. Ed.* **57**, 7709–7713 (2018).
47. V. Andrushchenko, H. Vogel, E. Prenner, Solvent-dependent structure of two tryptophan-rich antimicrobial peptides and their analogs studied by FTIR and CD spectroscopy. *Biochim. Biophys. Acta Biomembr.* **1758**, 1596–1608 (2006).
48. E. T. Pashuck, H. Cui, S. I. Stupp, Tuning supramolecular rigidity of peptide fibers through molecular structure. *J. Am. Chem. Soc.* **132**, 6041–6046 (2010).
49. E. L. Bakota, Y. Wang, F. R. Danesh, J. D. Hartgerink, Injectable multidomain peptide nanofiber hydrogel as a delivery agent for stem cell secretome. *Biomacromolecules* **12**, 1651–1657 (2011).
50. S. Bera, S. Mondal, Y. Tang, G. Jacoby, E. Arad, T. Guterman, R. Jelinek, R. Beck, G. Wei, E. Gazit, Deciphering the rules for amino acid co-assembly based on interlayer distances. *ACS Nano* **13**, 1703–1712 (2019).
51. J. P. Gallivan, D. A. Dougherty, Cation-π interactions in structural biology. *Proc. Natl. Acad. Sci. U.S.A.* **96**, 9459–9464 (1999).
52. R. Zhao, R.-Q. Zhang, A new insight into π-π stacking involving remarkable orbital interactions. *Phys. Chem. Chem. Phys.* **18**, 25452–25457 (2016).
53. U. Samanta, D. Pal, P. Chakrabarti, Packing of aromatic rings against tryptophan residues in proteins. *Acta Crystallogr. D Biol. Crystallogr.* **55**, 1421–1427 (1999).
54. H. Dong, S. E. Paramonov, L. Aulisa, E. L. Bakota, J. D. Hartgerink, Self-assembly of multidomain peptides: Balancing molecular frustration controls conformation and nanostructure. *J. Am. Chem. Soc.* **129**, 12468–12472 (2007).
55. K. Wong, Y. Wang, D. Seroski, G. Larkin, A. Mehta, G. Hudalla, C. Hall, A. Paravastu, Molecular complementarity and structural heterogeneity within co-assembled peptide β-sheet nanofibers. *Nanoscale* **12**, 4506–4518 (2020).
56. T. Yu, O.-S. Lee, G. C. Schatz, Steered molecular dynamics studies of the potential of mean force for peptide amphiphile self-assembly into cylindrical nanofibers. *J. Phys. Chem. A* **117**, 7453–7460 (2013).
57. J. J. de Pablo, N. E. Jackson, M. A. Webb, L.-Q. Chen, J. E. Moore, D. Morgan, R. Jacobs, T. Pollock, D. G. Schlom, E. S. Toberer, J. Analytis, I. Dabo, D. M. DeLongchamp, G. A. Fiete, G. M. Grason, G. Hautier, Y. Mo, K. Rajan, E. J. Reed, E. Rodriguez, V. Stevanovic, J. Suntivich, K. Thornton, J.-C. Zhao, New frontiers for the materials genome initiative. *Npj Comput. Mater.* **5**, 1–23 (2019).
58. J. Sadownik, J. Leckie, R. Ulijn, Micelle to fibre biocatalytic supramolecular transfor-mation of an aromatic peptide amphiphile. *Chem. Commun.* **47**, 728–730 (2010).
59. M. J. Abraham, T. Murtola, R. Schulz, S. Páll, J. C. Smith, B. Hess, E. Lindahl, GROMACS: High performance molecular simulations through multi-level parallelism from laptops to supercomputers. *SoftwareX* **1-2**, 19–25 (2015).
60. E. Lindahl, B. Hess, D. van der Spoel, GROMACS 3.0: A package for molecular simulation and trajectory analysis. *J. Mol. Model.* **7**, 306–317 (2001).
61. S. Páll, M. J. Abraham, C. Kutzner, B. Hess, E. Lindahl, *Tackling Exascale Software Challenges in Molecular Dynamics Simulations with GROMACS* (Springer, 2015), pp. 3–27.
62. H. Berendsen, D. van der Spoel, R. van Drunen, GROMACS: A message-passing parallel molecular dynamics implementation. *Comput. Phys. Commun.* **91**, 43–56 (1995).
63. D. V. D. Spoel, E. Lindahl, B. Hess, G. Groenhof, A. E. Mark, H. J. C. Berendsen, GROMACS: Fast, flexible, and free. *J. Comput. Chem.* **26**, 1701–1718 (2005).
64. S. Pronk, S. Páll, R. Schulz, P. Larsson, P. Bjelkmar, R. Apostolov, M. R. Shirts, J. C. Smith, P. M. Kasson, D. van der Spoel, B. Hess, E. Lindahl, GROMACS 4.5. *Bioinformatics* **29**, 845–854 (2013).
65. A. Lindahl, S. V. Hess, D. van der Spoel, GROMACS 2020.3 source code (2020).
66. O. Beckstein, GromacsWrapper (2017).
67. A. D. MacKerell Jr., D. Bashford, M. Bellott, R. L. Dunbrack Jr., J. D. Evanseck, M. J. Field, S. Fischer, J. Gao, H. Guo, S. Ha, D. Joseph-McCarthy, L. Kuchnir, K. Kuczera, F. T. K. Lau, C. Mattos, S. Michnick, T. Ngo, D. T. Nguyen, B. Prodhom, W. E. Reiher, B. Roux, M. Schlenkrich, J. C. Smith, R. Stote, J. Straub, M. Watanabe, J. Wiórkiewicz-Kuczera, D. Yin, M. Karplus, All-atom empirical potential for molecular modeling and dynamics studies of proteins. *J. Phys. Chem. B* **102**, 3586–3616 (1998).
68. A. D. Mackerell Jr., M. Feig, C. L. Brooks III, Extending the treatment of backbone energetics in protein force fields: Limitations of gas-phase quantum mechanics in reproducing protein conformational distributions in molecular dynamics simulations. *J. Comput. Chem.* **25**, 1400–1415 (2004).
69. G. Bussi, D. Donadio, M. Parrinello, Canonical sampling through velocity rescaling. *J. Chem. Phys.* **126**, 014101 (2007).
70. U. Essmann, L. Perera, M. L. Berkowitz, T. Darden, H. Lee, L. G. Pedersen, A smooth particle mesh ewald method. *J. Chem. Phys.* **103**, 8577–8593 (1995).

71. B. Hess, H. Bekker, H. J. C. Berendsen, J. G. E. M. Fraaije, LINCS: A linear constraint solver for molecular simulations. *J. Comput. Chem.* **18**, 1463–1472 (1997).
72. M. Z. Tien, D. K. Sydykova, A. G. Meyer, C. O. Wilke, Peptidebuilder: A simple Python library to generate model peptides. *PeerJ* **1**, e80 (2013).
73. L. Martínez, R. Andrade, E. G. Birgin, J. M. Martínez, Packmol: A package for building initial configurations for molecular dynamics simulations. *J. Comput. Chem.* **30**, 2157–2164 (2009).
74. N. Thota, Z. Luo, Z. Hu, J. Jiang, Self-assembly of amphiphilic peptide (af) 6h5k15: Coarse-grained molecular dynamics simulation. *J. Phys. Chem. B* **117**, 9690–9698 (2013).
75. G. A. Tribello, M. Bonomi, D. Branduardi, C. Camilloni, G. Bussi, Plumed 2: New feathers for an old bird. *Comput. Phys. Commun.* **185**, 604–613 (2014).
76. M. Bonomi, G. Bussi, C. Camilloni, G. A. Tribello, P. Banáš, A. Barducci, M. Bernetti, P. G. Bolhuis, S. Bottaro, D. Branduardi, R. Capelli, P. Carloni, M. Ceriotti, A. Cesari, H. Chen, W. Chen, F. Colizzi, S. De, M. De La Pierre, D. Donadio, V. Drobot, B. Ensing, A. L. Ferguson, M. Filizola, J. S. Fraser, H. Fu, P. Gasparotto, F. L. Gervasio, F. Giberti, A. Gil-Ley, T. Giorgino, G. T. Heller, G. M. Hocky, M. Iannuzzi, M. Invernizzi, K. E. Jelfs, A. Jussupow, E. Kirilin, A. Laio, V. Limongelli, K. Lindorff-Larsen, T. Löhr, F. Marinelli, L. Martin-Samos, M. Masetti, R. Meyer, A. Michaelides, C. Molteni, T. Morishita, M. Nava, C. Paissoni, E. Papaleo, M. Parrinello, J. Pfaendtner, P. Piaggi, G. M. Piccini, A. Pietropaolo, F. Pietrucci, S. Pipolo, D. Provasi, D. Quigley, P. Raiteri, S. Raniolo, J. Rydzewski, M. Salvalaglio, G. C. Sosso, V. Spiwok, J. Šponer, D. W. H. Swenson, P. Tiwary, O. Valsson, M. Vendruscolo, G. A. Voth, A. White, Promoting transparency and reproducibility in enhanced molecular simulations. *Nat. Methods* **16**, 670–673 (2019).
77. R. T. McGibbon, K. A. Beauchamp, M. P. Harrigan, C. Klein, J. M. Swails, C. X. Hernández, C. R. Schwantes, L.-P. Wang, T. J. Lane, V. S. Pande, Mdtraj: A modern open library for the analysis of molecular dynamics trajectories. *Biophys. J.* **109**, 1528–1532 (2015).
78. M. Bonomi, M. Parrinello, Enhanced sampling in the well-tempered ensemble. *Phys. Rev. Lett.* **104**, 190601 (2010).
79. A. Barducci, G. Bussi, M. Parrinello, Well-tempered metadynamics: A smoothly converging and tunable free-energy method. *Phys. Rev. Lett.* **100**, 020603 (2008).
80. A. Laio, M. Parrinello, Escaping free-energy minima. *Proc. Natl. Acad. Sci. U.S.A.* **99**, 12562–12566 (2002).

Acknowledgments: We thank J. Grime for comments and discussions of our results and G. Hocky for discussions. **Funding:** This work was supported by the NSF under grant 1751471 and, in part, by the Oklahoma Tobacco Settlement Endowment Trust awarded to the University of Oklahoma, Stephenson Cancer Center and by a grant from the Research Council of the University of Oklahoma Norman Campus. The content is solely the responsibility of the authors and does not necessarily represent the official views of the Oklahoma Tobacco Settlement Endowment Trust. **Author contributions:** H.A. designed and supervised research. S.H. performed experimental analyses and collected data. A.D.W. designed the computational simulations and performed and analyzed data. H.A., S.H., and A.D.W. wrote the paper. **Competing interests:** The authors declare that they have no competing interests. **Data and materials availability:** All data needed to evaluate the conclusions in the paper are present in the paper and/or the Supplementary Materials.

Submitted 16 April 2021
Accepted 22 November 2021
Published 19 January 2022
10.1126/sciadv.abj0305

ScienceAdvances

Peptide framework for screening the effects of amino acids on assembly

Seren HamsiciAndrew D. WhiteHandan Acar

Sci. Adv., 8 (3), eabj0305. • DOI: 10.1126/sciadv.abj0305

Science Advances (ISSN) is published by the American Association for the Advancement of Science. 1200 New York Avenue NW, Washington, DC 20005. The title *Science Advances* is a registered trademark of AAAS.